Optics Letters

Simplified read schemes for krypton tagging velocimetry in N₂ and air

M. A. Mustafa [ID] **and N. J. Parziale*** [ID]

Mechanical Engineering, Stevens Institute of Technology, 1 Castle Point on Hudson, Hoboken, New Jersey 07030, USA
Corresponding author: nick.parziale@gmail.com

The background and results for two simplified read schemes for krypton tagging velocimetry (KTV) are presented. The first scheme utilizes the excitation/re-excitation approach found in the literature but replaces the pulsed dye laser used for the re-excitation step with a continuous wave, narrowband laser diode. The second scheme is a single-laser setup with no read laser where the fluorescence of the tagged Kr is imaged at successive times. Results are presented and compared to historical data for experiments performed in 99%N₂/1% Kr and 95% air/5% Kr underexpanded jets. The approach with the laser diode has a higher signal, while the single-laser approach yields more consistent results. Both schemes maintain an SNR comparable to that in the literature, but with a simpler setup that enables future high-repetition rate KTV experiments. © 2018 Optical Society of America

Advanced, nonintrusive instrumentation is currently being developed to supplement current measurement capabilities in combustion and supersonic/hypersonic flows. These efforts will help researchers improve their understanding of flow physics in harsh environments by probing previously inaccessible flow regimes for the purposes of model development (e.g., validation data for direct numerical simulation) and large-scale systems risk reduction (e.g., Test & Evaluation facility characterization).

Recently, researchers have used krypton as a tracer species for diagnostics because it is nominally thermochemically inactive at atmospheric or typical high-speed wind tunnel flow conditions. As such, it is safe/simple to implement in the lab, and it does not distort the mean flow of interest when introduced in dilute concentrations. That is, there is the potential for implementation in flows where the thermochemical state of the gas is difficult to prescribe or predict (e.g., a combustion environment or when introduced in the high-temperature/pressure reservoir of a high-speed wind tunnel).

The key to the use of Kr as a tracer species for diagnostics is the two-photon transitions that are accessible with commercially available optics and laser systems; there are several two-photon transitions in the ≈190–220 nm range. Kr-planar laser-induced fluorescence (K-PLIF) with nanosecond dye lasers has been used to image scalars in supersonic flows [1], perform mixture-fraction studies in turbulent nonpremixed flames [2], and perform composition-independent mean temperature measurements in laminar diffusion flames [3]. In addition, the application of recently developed ultrafast laser technology to Kr-based diagnostics is promising because of the high-repetition rate and intensity. Researchers have used ultrafast K-PLIF to image developing Kr jets [4] and mixture-fraction imaging comparing many K-PLIF excitation wavelengths [5].

In this work, we focus on the use of Kr as a tracer for tagging velocimetry. Tagging velocimetry's advantage over particle-based techniques is that it is not limited by issues associated with tracer injection or reduced particle response at Knudsen and Reynolds numbers characteristic of high-speed wind tunnels. Other methods of tagging velocimetry include the VENOM [6], APART [7], RELIEF [8], FLEET [9], STARFLEET [10], PLEET [11], and N₂O [12], among others [13].

The use of a metastable noble gas as a tagging velocimetry tracer was first suggested by Mills *et al.* [14] and Balla and Everheart [15]. To date, krypton tagging velocimetry (KTV) has been demonstrated by globally seeding high-speed N₂ flows with 1% Kr. Applications include 1) an underexpanded jet (first KTV demonstration) [16], 2) mean and fluctuating turbulent boundary-layer profiles in a Mach 2.7 flow [17], 3) seven simultaneous profiles of streamwise velocity and velocity fluctuations in a Mach 2.8 shock wave/turbulent boundary-layer interaction [18], and 4) in the freestream of the large-scale AEDC hypervelocity tunnel 9 at Mach 10 and Mach 14 [19]. In these experiments, the researchers used a pulsed dye laser to perform the write step at 214.7 nm to form a write line and photosynthesize the metastable Kr tracer; after a prescribed delay, an additional pulsed dye laser is used to re-excite the metastable Kr tracer to track displacement.

In this Letter, we present two alternate read schemes for KTV that reduce complexity and cost. The first new read scheme utilizes the excitation/re-excitation approach found in the literature [19] but replaces the pulsed dye laser used for the re-excitation step with a single-frequency, continuous
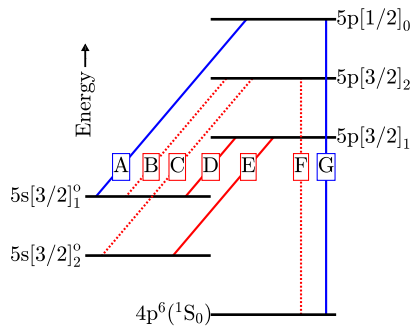
Fig. 1. Energy diagram. Racah nl[K]$_J$ notation. Scheme marked in red utilizes conventional 214.7 nm excitation with re-excitation by laser diode at 769.7 nm. Scheme marked in blue uses excitation at 212.56 nm with successive camera gating (no read laser). Transition details in Table 1.

wave laser diode. The second scheme is a single-laser setup with no read laser where the fluorescence of the tagged Kr is imaged at successive times. For both simplified read schemes, we present sample results in an underexpanded jet of N_2 and air doped with 1% and 5% Kr, respectively.

Following the transitions marked in red in the energy level diagram in Fig. 1 along with the relevant transition data in Table 1 (labeled as A, B, etc.), the first new KTV scheme is performed as follows:

1. **Write Step:** photosynthesize metastable krypton atoms with a pulsed tunable laser to form the tagged tracer: two-photon excitation of $4p^6(^1S_0) \rightarrow 5p[3/2]_2$ (214.7 nm, F) and decay to resonance state $5p[3/2]_2 \rightarrow 5s[3/2]_1^o$ (819.2 nm, B) and metastable state $5p[3/2]_2 \rightarrow 5s[3/2]_2^o$ (760.4 nm, C). A camera positioned normal to the flow records the position of the write line by gated imaging of the lase- induced fluorescence (LIF) from these transitions.

2. **Read Step:** at a prescribed delay, record the displacement of the tagged metastable krypton by gated imaging of the LIF that is produced with an additional tunable laser: excite $5p[3/2]_1$ level by $5s[3/2]_2^o \rightarrow 5p[3/2]_1$ transitions with laser sheet (769.7 nm, E) and read spontaneous emission of $5p[3/2]_1 \rightarrow 5s[3/2]_1^o$ (830.0 nm, D) and $5p[3/2]_1 \rightarrow 5s[3/2]_2^o$ (769.7 nm, E) transitions.

The above scheme is the same as that in the literature, except that in this work the read step is performed with a single-frequency, continuous wave laser diode. Although this scheme is technically still a two-laser, one-camera technique, the barrier to entry for implementation is significantly reduced.

The second new KTV scheme is a one-laser, one-camera velocimetry technique. Following the transitions marked in blue in Fig. 1 and the data in Table 1, it is performed as follows:

1. **Write Step:** Excite krypton atoms with a pulsed tunable laser to form the tagged tracer: two-photon excitation of $4p^6(^1S_0) \rightarrow 5p[1/2]_0$ (212.6 nm, G) and decay to resonance state $5p[1/2]_0 \rightarrow 5s[3/2]_1^o$ (758.9 nm, A). The position of the write line is marked by gated imaging of the LIF from these transitions, recorded with a camera positioned normal to the flow.

2. **Read Step:** At a prescribed delay, record the displacement of the tagged krypton by gated imaging the LIF from the residual $5p[1/2]_0 \rightarrow 5s[3/2]_1^o$ (758.9 nm, A) transitions.

The 212.6 nm two-photon transition is chosen because, in contrast to the other two-photon transitions in Kr, there is only one 5 p to 5 s transition that may be quenched. This is potentially the reason why researchers found a relatively high K-PLIF signal for the 212.6 nm transition as opposed to others [5].

To demonstrate the new KTV schemes, an underexpanded jet was used as the flow field (schematic in Fig. 2). The jet was exhausted into a test cell that was maintained at approximately 5 torr (orifice diameter of $D_j = 2$ mm). A gas pressure regulator was used to control the effective plenum pressure of the underexpanded jet, and a high-speed solenoid was used to pulse the jet for 20 ms, beginning 15 ms prior to the write laser pulse (jet flow establishment time is estimated to be 5 ms [20]). Two mixtures were used in this work: 99%N_2/1%Kr and 75%N_2/20%O_2/5%Kr (K-bottles from Praxair). To assess the effect of Kr doping on the flow properties, an empirical fit was used to calculate the Mach number [21], and the transport properties were calculated using Cantera [22]. The properties at $x/D_j = 2$ are presented in Table 2, including Kr-doped and undoped jet properties with a comparison in percent difference. Doping the air jet with 5% Kr does alter the density appreciably (12.4%). However, the properties most important for scientific study are the nondimensional flow properties; these change due to Kr doping by a modest 0.2%–1.3%, are calculable (e.g., with Cantera), and are ultimately appropriate for scientific study.

The write laser system is a frequency-doubled Quanta Ray Pro-350 Nd:YAG laser and a frequency-tripled Sirah PrecisionScan dye laser (DCM dye, DMSO solvent). The Nd:YAG laser pumped the dye laser with a 500 mJ/pulse at a wavelength of 532 nm. The dye laser was tuned to output a 644.1 or 637.7 nm beam, and frequency tripling (Sirah THU 205) of the dye laser output resulted in a 214.7 or 212.6 nm beam with 5 mJ energy, 1350 MHz linewidth, 7 ns pulse width, at a repetition rate of 10 Hz. The write beam was focused to four narrow waists in the test section with a

Table 1.   Relevant NIST Atomic Spectra Database Lines Data; Labels Match Fig. 1[a]

| Transition	λ_{vac}(nm)	Nature	A_{ki} (1/s)	E_i(cm^{-1})	E_k(cm^{-1})	Lower Level	Upper Level
A	758.950	single-photon	5.1e7	80916.7680	94092.8626	$5s[3/2]_1^o$	$5p[1/2]_0$
B	819.230	single-photon	1.1e7	80916.7680	93123.3409	$5s[3/2]_1^o$	$5p[3/2]_2$
C	760.364	single-photon	3.1e7	79971.7417	93123.3409	$5s[3/2]_2^o$	$5p[3/2]_2$
D	830.039	single-photon	3.2e7	80916.7680	92964.3943	$5s[3/2]_1^o$	$5p[3/2]_1$
E	769.666	single-photon	5.6e6	79971.7417	92964.3943	$5s[3/2]_2^o$	$5p[3/2]_1$
F	214.769	two-photon		0	93123.3409	$4s^2 4p^6, {}^1S_0$	$5p[3/2]_2$
G	212.556	two-photon		0	94092.8626	$4s^2 4p^6, {}^1S_0$	$5p[1/2]_2$

[a]Racah nl[K]$_J$ notation.
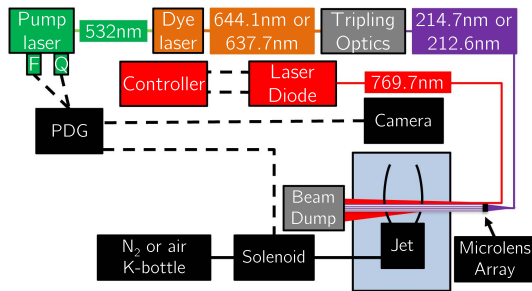
Fig. 2. Schematic of experimental setup.

fused-silica, $f = 100$ mm microlens array. The beam fluence and spectral intensity at each beam waist was approximately 54 J/cm^2 and 5.6 W/(cm^2 Hz).

The read laser is a single-frequency, continuous wave laser diode (Photodigm-PH770DBR) with current and temperature monitored by a Thorlabs controller. The free space output beam had ≈ 80 mW power at 769.7 nm wavelength and 1 MHz linewidth, which were monitored with a wavemeter (HighFinesse WS6). Optics were used to turn and focus the laser diode output to a sheet of approximate dimensions 10 mm × 1 mm. The spectral intensity was approximately 8 mW/(m^2 Hz). For context, the linewidth of transition E is ≈ 500 MHz, so the laser diode bandwidth was sufficiently narrow.

The intensified camera used for all experiments was a Princeton Instruments PIMAX-4 (PM4-1024i-HR-FG-18-P46-CM) with a Nikon NIKKOR 24–85 mm $f/2.8$–$4D$ lens in "macro" mode and positioned approximately 200 mm from the write/read location. The gain was set to 100% with 2 × 2 pixel binning. For the first scheme, the camera gate was opened for 50 ns immediately following the write laser pulse to capture the 819.2 nm (B) and 760.3 nm (C) transitions, and again after a prescribed delay, to capture the 830.0 nm (D) and 769.7 nm (E) transitions. For the second scheme, the camera gate was opened twice for 50 ns immediately following the write laser pulse and again at a prescribed delay time to capture the 758.9 nm (A) transitions.

In Fig. 3, we present single-shot KTV exposures for the 99%N_2/1% Kr underexpanded jet for write/read delays from $\Delta t = 0$ to $\Delta t = 3000$ ns. The top four frames used the first new KTV read scheme: the write step performed by two-photon excitation at 214.7 nm and the read step done with the laser diode at 769.7 nm. The bottom four frames were performed with the single-laser strategy with the two-photon excitation at 212.56 nm. These exposures are of similar SNR and similar write/read delay as the initial KTV experiments

Table 2. Conditions of the Underexpanded Jet at $x/D_j = 2$

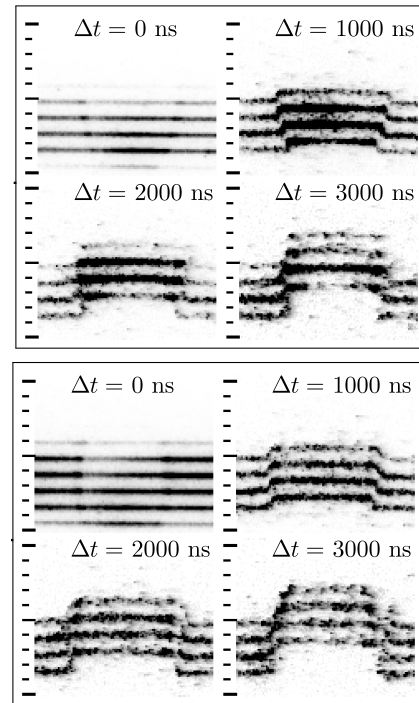| Gas Composition (Mole fraction)	M_j (–)	Re_j^{unit} (1/m)	Pr (–)	γ (–)	P_j (Pa)	T_j (K)	ρ_j (g/m^3)
1.N$_2$	5.00	89.0e6	0.709	1.40	378	49.1	25.9
.99N$_2$/.01Kr%	5.01	88.9e6	0.707	1.40	379	48.9	26.6
% change	0.1%	0.2%	0.2%	0.1%	0.3%	0.4%	2.8%
.78N$_2$/.21O$_2$/.01Ar	5.00	89.2e6	0.710	1.40	378	49.0	26.9
.75N$_2$/.20O$_2$/.05Kr	5.01	88.4e6	0.702	1.41	383	48.2	30.2
% change	0.2%	0.9%	1.2%	0.5%	1.3%	1.7%	12.4%

Fig. 3. Single-shot fluorescence exposures for 99%N_2/1% Kr jet experiments with laser diode (top four) and single-laser scheme (bottom four). Tick marks are 1 mm. Flow is bottom to top. Inverted intensity scale.

performed in N_2/Kr underexpanded jets by Parziale et al. [16], where the read step was performed with a pulsed dye laser.

In Fig. 4 we present the first KTV experiments in air as single-shot KTV exposures for the 95% air/5% Kr underexpanded jet for write/read delays from $\Delta t = 0$ to $\Delta t = 1000$ ns. The presence of O_2 requires the shorter write/read delay and larger doping fraction of Kr because it effectively quenches the metastable state [23] for the two-laser scheme and quenches the 758.9 nm transitions in the single-laser scheme.

The mean and standard deviation of the signal-to-noise ratio (SNR) for the middle two of the four tagged Kr lines (refer to Figs. 3 and 4) are computed for 25 experiments of each gas and write/read delay. The results are presented in Fig. 5 to compare the SNR and consistency of the two new read strategies. The
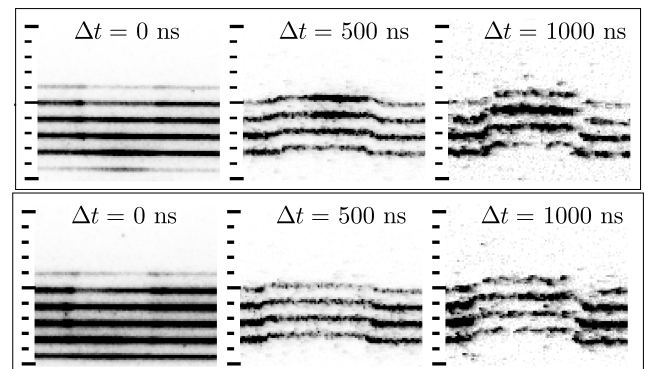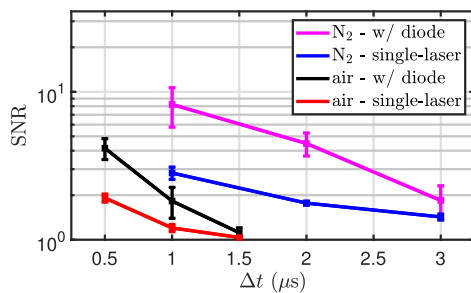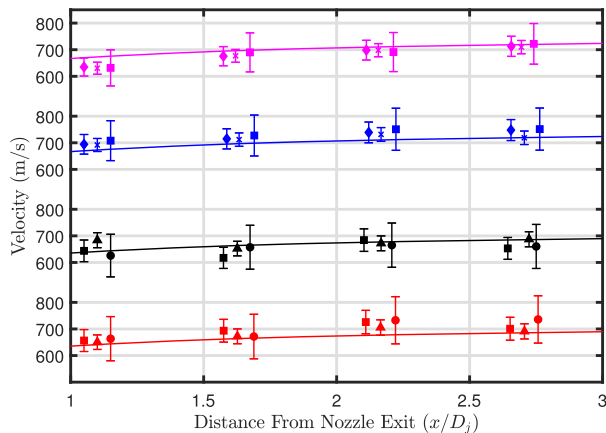

Fig. 4. Single-shot fluorescence exposures for 95% air/5% Kr jet experiments with laser diode (top) and single-laser scheme (bottom). Tick marks are 1 mm. Flow is bottom to top. Inverted intensity scale.

Fig. 5. Mean SNR versus delay for underexpanded jet experiments. Error bars represent the standard deviation of SNR.

Fig. 6. Measured underexpanded jet velocity. Legend in Fig. 5. Error bars represent uncertainty estimate. Write/read delay times are denoted by circle, square, triangle, diamond, and x for 500, 1000, 1500, 2000, and 3000 ns, respectively.

SNR is higher for the first new KTV scheme utilizing the two-photon excitation at 214.7 nm and re-excitation at 769.7 nm via the laser diode. However, more consistent results (lower standard deviation) are obtained via the single-laser scheme via two-photon excitation at 212.56 nm and successive gating. SNR is important, but in supersonic turbulent flows, signal-count consistency increases the effectiveness of tagged-line tracking algorithms dependent on initial line location guesses [17,18].

The measured velocity results for each case, which are found via Gaussian fitting along the jet centerline (5 pixel spanwise average), are presented in Fig. 6. Uncertainty is treated in the same way as in Parziale *et al.* [16], with the spatial and temporal uncertainty estimated to be 25 microns (data fitting) and 50 ns (camera gate), respectively. The solid lines represent calculations of velocity from empirical fits for the Mach number [21]. Note the slight difference in dimensional velocity in the N_2 versus the air jet due to the slight change in local sound speed.

In summary, we have presented two new read schemes for KTV and demonstrated them in underexpanded jets comprised of 99%N_2/1% Kr versus 95% air/5% Kr. The experiments in the N_2 jet are of comparable SNR, write/read delay, and gas composition as the initial KTV experiments in the literature [16], where the read step was performed with a pulsed dye laser. The experiments performed in air are the first of their kind, to

the best of our knowledge. The new read schemes significantly reduce the complexity and cost of the KTV technique and enable the possibility of high-repetition rate KTV with existing or slightly modified technology. Data in the literature suggests that the write step could be performed by ultrafast lasers [5] or a tunable form of a burst-mode laser [24]. Finally, the laser diode used for the current experiments was a relatively low-powered (80 mW) single-frequency laser diode with a beam profile typical of such. Coupling this diode or similar to a tapered amplifier would yield a further increase in SNR (increased power) and also shot-to-shot consistency (increased beam profile quality).

REFERENCES

1. V. Narayanaswamy, R. Burns, and N. T. Clemens, Opt. Lett. **36**, 4185 (2011).
2. A. G. Hsu, V. Narayanaswamy, N. T. Clemens, and J. H. Frank, Proc. Combust. Inst. **33**, 759 (2011).
3. D. Zelenak and V. Narayanaswamy, Exp. Fluids **58**, 147 (2017).
4. Y. Wang, C. Capps, and W. D. Kulatilaka, Opt. Lett. **42**, 711 (2017).
5. D. R. Richardson, N. Jiang, H. U. Stauffer, S. P. Kearney, S. Roy, and J. R. Gord, Opt. Lett. **42**, 3498 (2017).
6. A. G. Hsu, R. Srinivasan, R. D. W. Bowersox, and S. W. North, AIAA J. **47**, 2597 (2009).
7. N. Dam, R. J. H. Klein-Douwel, N. M. Sijtsema, and J. J. ter Meulen, Opt. Lett. **26**, 36 (2001).
8. R. Miles, C. Cohen, J. Connors, P. Howard, S. Huang, E. Markovitz, and G. Russell, Opt. Lett. **12**, 861 (1987).
9. J. B. Michael, M. R. Edwards, A. Dogariu, and R. B. Miles, Appl. Opt. **50**, 5158 (2011).
10. N. Jiang, B. R. Halls, H. U. Stauffer, P. M. Danehy, J. R. Gord, and S. Roy, Opt. Lett. **41**, 2225 (2016).
11. N. Jiang, J. G. Mance, M. N. Slipchenko, J. J. Felver, H. U. Stauffer, T. Yi, P. M. Danehy, and S. Roy, Opt. Lett. **42**, 239 (2017).
12. M. A. André, R. A. Burns, P. M. Danehy, S. R. Cadell, B. G. Woods, and P. M. Bardet, Exp. Fluids **59**, 14 (2018).
13. M. A. André, P. M. Bardet, R. A. Burns, and P. M. Danehy, Meas. Sci. Technol. **28**, 085202 (2017).
14. J. L. Mills, C. I. Sukenik, and R. J. Balla, in *Proceedings of 42nd AIAA Plasmadynamics and Lasers Conference*, Honolulu, Hawaii, 2011, paper AIAA 2011-3459.
15. R. J. Balla and J. L. Everhart, AIAA J. **50**, 698 (2012).
16. N. J. Parziale, M. S. Smith, and E. C. Marineau, Appl. Opt. **54**, 5094 (2015).
17. D. Zahradka, N. J. Parziale, M. S. Smith, and E. C. Marineau, Exp. Fluids **57**, 62 (2016).
18. M. A. Mustafa, M. B. Hunt, N. J. Parziale, M. S. Smith, and E. C. Marineau, in *Proceedings of AIAA SciTech 2017*, Grapevine, Texas, 2017, paper AIAA 2017-0025.
19. M. A. Mustafa, N. J. Parziale, M. S. Smith, and E. C. Marineau, AIAA J. **55**, 3611 (2017).
20. C. E. Smith, Int. J. Fluid Mech. Res. **24**, 625 (1966).
21. S. Crist, D. R. Glass, and P. M. Sherman, AIAA J. **4**, 68 (1966).
22. D. G. Goodwin, in *Proceedings of CVD XVI and EuroCVD Fourteen,*" M. Allendorf, F. Maury, and F. Teyssandier, eds. (2003), pp. 155–162.
23. J. E. Velazco, J. H. Kolts, and D. W. Setser, J. Chem. Phys. **69**, 4357 (1978).
24. M. N. Slipchenko, J. D. Miller, S. Roy, J. R. Gord, S. A. Danczyk, and T. R. Meyer, Opt. Lett. **37**, 1346 (2012).